HHS Public Access

Author manuscript

Nat Immunol. Author manuscript; available in PMC 2016 May 01.

Published in final edited form as:

Nat Immunol. 2015 November ; 16(11): 1185–1194. doi:10.1038/ni.3292.

MicroRNA-22 Inhibits Histone Deacetylase 4 to Promote T Helper-17 Cell-Dependent Emphysema

Wen Lu[1], **Ran You**[1], **Xiaoyi Yuan**[1], **Tianshu Yang**[2], **Errol L. G. Samuel**[3], **Daniela C. Marcano**[3], **William K. A. Sikkema**[3], **James M. Tour**[3], **Antony Rodriguez**[4], **Farrah Kheradmand**[1,2,5,6], and **David B. Corry**[1,2,5,6]

[1]Department of Pathology & Immunology, Baylor College of Medicine, Houston, TX, USA, 77030

[2]Translational Biology and Molecular Medicine Program, Baylor College of Medicine, Houston, TX, USA, 77030

[3]Department of Chemistry, Rice University, Houston, Texas, USA, 77005

[4]Department of Human and Molecular Genetics, Baylor College of Medicine, Houston, TX, USA, 77030

[5]Department of Medicine, Baylor College of Medicine, Houston, TX, USA, 77030

[6]Biology of Inflammation Center and the Michael E. DeBakey VA Center for Translational Research on Inflammatory Diseases, Houston, Texas, USA, 77030

Abstract

Smoking-related emphysema is a chronic inflammatory disease driven by T helper 17 (T_H17) cells through molecular mechanisms that remain obscure. Here we have explored the role of microRNA-22 (miR-22) in emphysema. MiR-22 was upregulated in lung myeloid dendritic cells (mDCs) of smokers with emphysema and antigen-presenting cells (APCs) of mice exposed to smoke or nanoparticulate carbon black (nCB) through a mechanism involving NF-κB. MiR-22-deficient mice, but not wild-type, showed attenuated T_H17 responses and failed to develop emphysema after exposure to either smoke or nCB. We further show that miR-22 controls APC activation and T_H17 responses through activation of AP-1 transcription factor complexes and histone deacetylase (HDAC) 4. Thus, miR-22 is a critical regulator of both emphysema and T_H17 responses.

Correspondence should be addressed to D.B.C. (dcorry@bcm.edu) or F.K. (farrahk@bcm.edu). One Baylor Plaza Suite M915D BCM285, Houston, TX 77030, Tele: 713 798 8740; 713-798-8622.

*Present address: Department of Physical Therapy, University of Texas Medical Branch Galveston, 301 University Boulevard, Galveston, TX 77555, USA

Accession codes for Illumina microarray gene expression: GSE72734

AUTHOR CONTRIBUTIONS

W.L. and D.B.C. conceptualized the project and all studies. W.L. designed and performed all experiments with R.Y., X.Y. and T.Y. contributing to selected mouse experiments and micro-CT analysis. E.L.G.S., D.C.M., W.K.A.S. and J.T. prepared nCB. A.R. provided miR-22 deficient mice. F.K. and D.B.C. provided grant support. W.L. and D.B.C. wrote the manuscript with assistance from all co-authors.

COMPETING FINANCIAL INTERESTS

The authors declare no competing financial interests.

Pulmonary emphysema is a chronic inflammatory lung condition that, together with other smoking-related chronic obstructive pulmonary diseases (COPD), represents the third leading cause of death in United States[1]. Emphysema is characterized by the disruption of lung matrix support that leads to the enlargement and destruction of the primary gas exchange units of the lung, the alveoli, and enhanced collapsibility of conducting airways. These pathological changes, which are often accompanied by loss of the pulmonary microvasculature, combine to severely limit gas exchange and exercise tolerance. Emphysema is further the most predictive clinical marker of lung cancer, the most deadly malignancy of industrialized societies[2]. Although tobacco smoking is the most important risk factor, emphysema is also seen in tobacco non-users who are chronically exposed to smoke derived from other sources[3].

Susceptible smokers harbor activated T helper type 1 (T_H1) and T_H17 cells in their lungs and circulating elastin-specific autoimmune T cells have been cloned from the peripheral blood of smokers[4]. Elastin is the major structural protein of lung that tethers the airways open during exhalation and accelerated loss of this matrix protein through the enhanced activity of elastases largely accounts for the dynamic airway collapse and lung hyperinflation that are characteristic of emphysema. Interferon-γ (IFN-γ) and interleukin 17A (IL-17A), the canonical T_H1 and T_H17 cytokines, respectively, either promote elastase secretion from constitutive lung cells directly or indirectly by promoting secretion of chemokines such as KC and macrophage inflammatory proteins that drive the recruitment of elastase-secreting neutrophils and macrophages to lung[5,6]. However, the mechanism underlying the loss of peripheral tolerance to self-antigens such as elastin and induction of autoreactive T_H1 and T_H17 cells by cigarette smoke remains unclear.

We have previously shown that central to the development of these pathogenic T cells are lung $CD1a^+$ mDCs that assume a highly activated phenotype[6]. $CD1a^+$ mDCs from human smokers with emphysema and $CD11c^+$ APCs from mice exposed chronically to cigarette smoke induce T_H17 differentiation from syngeneic and allogeneic T cells through a mechanism that involves the production of the cytokines IL-6 and osteopontin and inhibition of the transcription factor peroxisome proliferator activated receptor gamma (PPAR-γ)[7,8]. Indeed, smoke-exposed APCs are alone sufficient to promote the development of emphysema upon adoptive transfer to mice[7]. However, little is currently understood about how cigarette smoke initiates lung DC activation and the initial smoke-activated molecular pathways that drive chronic inflammation and diseases such as emphysema.

MicroRNAs (miRNAs) represent a well-recognized layer of gene regulation that may critically influence immunological diseases such as emphysema. MiRNAs are endogenous small noncoding RNAs, approximately 23 nt in length, that post-transcriptionally regulate gene expression by binding to target sequences located within the 3′ untranslated regions (UTR) of select mRNAs. MiRNAs bind to 3′-UTR targets in association with argonaute proteins within the cytoplasmic RNA-induced silencing complex (RISC), leading to mRNA degradation or inhibition of translation. Over 100 miRNAs are selectively expressed in cells of the mammalian immune system, many of which have been linked to either normal immune responses or autoimmune disease[9]. We previously demonstrated that miRNAs of

the extended let-7 family are pro-inflammatory and promote the expression of allergic lung inflammation and disease that resembles allergic asthma[10].

During a screen of selected miRNAs for immunoregulatory activity, we discovered a potential pro-inflammatory role for miR-22. We show here that miR-22 is essential for the activation of DCs and expression of pulmonary emphysema resulting from the inhalation of cigarette smoke or nanoparticulate carbon black (nCB). Of the many miR-22 targets, the diverse immunological effects of miR-22 appear to be driven through a single major target, histone deacetylase 4, decreased expression of which leads to a highly-activated DC phenotype and robust T_H17 responses that drive pulmonary emphysema expression. Selective inhibition of miR-22 in the airway thus represents a novel and potentially effective therapy for diverse pulmonary and other inflammatory diseases.

Results

MiR-22 regulates cigarette smoke induced emphysema

To establish a potential relationship between miR-22 and human emphysema, we determined how miR-22 expression is regulated in lung mDCs from smokers with and without lung disease. As assessed by reverse transcription quantitative PCR (RT-qPCR), miR-22 expression in $CD1a^+$ lung mDCs from emphysema subjects was elevated in comparison to non-emphysema controls and positively correlated with obstructive airway disease severity as assessed by the forced expiratory volume in one second (FEV1) (Fig. 1a,b). We further examined the relationship between experimental emphysema in mice and miR-22 expression. Mice exposed to four months of cigarette smoke expressed significantly higher levels of miR-22 in $CD11c^+$ lung APCs as compared to air-exposed mice (Fig. 1c).

To determine if miR-22 is functionally implicated in emphysema pathogenesis, we initially compared the ability of wild-type and *Mir22*$^{-/-}$ mice to develop emphysema after four months of exposure to cigarette smoke. Wild-type mice exposed to smoke developed canonical features of emphysema including enlargement of the alveolar spaces and increased total lung volume accompanied by the accumulation of airway macrophages and neutrophils (Fig. 1d – g). In contrast, all emphysema-related parameters were either attenuated or abolished in *Mir22*$^{-/-}$ mice. Quantitation of lung T helper cell subsets specifically showed significantly fewer T_H17 cells in *Mir22*$^{-/-}$ mouse lung after smoke exposure (Fig. 1h). These data suggested miR-22 is required for the expression of cigarette smoke induced experimental emphysema.

Requirement of APC miR-22 in nCB-induced emphysema

Cigarette smoking leads to the deposition in lung of nCB, an insoluble substance that accumulates specifically in and activates APCs that promote pathological T_H1 and T_H17 responses and emphysema[11]. To determine a potential role for miR-22 in nCB-dependent inflammation, we further compared the ability of wild-type and *Mir22*$^{-/-}$ mice to develop emphysema after one month exposure to nCB. Wild-type and *Mir22*$^{-/-}$ mice were given nCB intranasally twice weekly for 6 weeks in amounts that approximate smokers' lung nCB burdens (0.1 mg/gm wet lung[11]). Four weeks following the last instillation of nCB, relative

to wild-type *Mir22*$^{-/-}$ mice exposed to nCB developed attenuated features of emphysema including less enlargement of the alveolar spaces and reduced total lung volume increases (Fig. 2a,b). Airway macrophage, neutrophil and T_H17 cell recruitment (Fig. 2c – e) and airway expression of the elastin degrading matrix metalloproteinases (MMPs) MMP9 and MMP2 were also reduced in *Mir22*$^{-/-}$ mice compared with wild-type mice (Supplementary Fig. 1a), while similar numbers of lung IL-17A$^+$ γδ$^+$ T cells were found (Supplementary Fig. 1b). We then immunized mice with ovalbumin and confirmed that miR-22 is selectively required for antigen-specific T_H17 cell, but not T_H1 or T_H2 cell, development *in vivo* (Supplementary Fig. 2).

Quantitation of cytokine production from mouse lung homogenates after nCB challenge further showed reduced secretion of IL-6, KC, MCP-1 and MIP-1â from *Mir22*$^{-/-}$ relative to wild-type mice (Supplementary Fig. 3a – d). Activated APCs are a principal cellular source of IL-6 (ref. [12]). To determine if APC activation and cytokine secretion is impaired in *Mir22*$^{-/-}$ mice, we isolated CD11c$^+$ APCs from nCB-challenged mice (Fig. 2a) and cultured overnight *ex vivo*. Isolated *Mir22*$^{-/-}$ APCs secreted significantly less IL-1β, IL-6, KC, MCP-1 and MIP-1β compared to wild-type APCs after nCB exposure (Fig. 2f,g; Supplementary Fig. 3e – g). nCB exposed *Mir22*$^{-/-}$ APCs were also less efficient at driving IL-17A secretion from wild-type T cells *in vitro* (Fig. 2h). To confirm that APC-specific miR-22 expression was selectively required for lung T_H17 responses and expression of emphysema, we generated mice with APC-specific *Mir22* deletion (*Mir22*^{CD11c}; *Mir22*$^{flox/flox}$ × CD11c-Cre). Similar to *Mir22*$^{-/-}$ mice, *Mir22*^{CD11c} mice developed attenuated macrophage and neutrophil infiltration into BALF and fewer lung T_H17 cells after nCB challenge compared with *Mir22*$^{flox/flox}$ mice (Fig. 2i – k). Furthermore, adoptive transfer of CD11c$^+$ lung APCs isolated from cigarette smoke-exposed wild-type mice induced emphysema, macrophage infiltration and lung T_H17 cell development in both naïve wild-type and *Mir22*$^{-/-}$ recipients (Supplementary Fig. 4). Together, these findings confirm that APC-specific miR-22 is necessary and sufficient for the induction of lung T_H17 responses and emphysema.

Transcriptional regulation of miR-22 through NF-κB

MiR-22 expression in human CD1a$^+$ mDCs and monocyte-derived dendritic cells (MoDCs) from non-emphysema subjects was enhanced after nCB exposure *ex vivo* (Fig. 3a,b). We observed similarly enhanced miR-22 expression in mouse bone marrow-derived dendritic cells (BMDCs) by a variety of activating stimuli including multiple Toll-like receptor (TLR) ligands and agonistic CD40 ligation in addition to nCB (Fig. 3c).

Expression of microRNAs typically correlates with that of the host genes from which they derive[13]. The miR-22 pri-miRNA host gene/transcription unit (*Mir22hg)* was also induced by nCB and several, but not all, TLR ligands (including lipopolysaccharide (LPS), FSL-1 (Pam2CGDPKHPKSF), poly(I:C), lipopeptide Pam_3CSK_4 and lipoteichoic acid) in mouse BMDCs (Fig. 3d). Ligation of CD40 using anti-CD40 conspicuously failed to induce *Mir22hg* expression, suggesting that the increase in mature miR-22 due to this form of stimulation may be the result of enhanced processing of extant *Mir22hg* transcripts or reduced consumption of miR-22. To understand how the *Mir22hg* is regulated in APCs, the

2.3-kb promoter region upstream of the *Mir22hg* transcriptional starting site was cloned into an eGFP reporter plasmid and multiple deletion mutants were generated and transfected into RAW264.7 cells. Both basal and stimulated (LPS, 1ng/ml), promoter activity progressively decreased as the promoter was shortened, suggesting that all regions of this promoter domain contain elements regulating *Mir22hg* expression (Fig. 3e).

TFSearch, a transcription factor binding site prediction server, predicts six potential AP-1 and one NF-κB consensus sequence within the *Mir22hg* 2.3-kb promoter region (Fig. 3e). To determine if *Mir22hg* promoter activity is regulated by AP-1 and NF-κB, RAW264.7 cells carrying a 2.3-kb *Mir22hg* promoter plasmid were treated with either a c-Jun N-terminal kinase (Jnk) inhibitor (SP600125) or MG132 to block AP-1 or NF-κB activity, respectively. MG132 significantly inhibited eGFP expression with and without LPS stimulation (Fig. 3f). Moreover, chromatin immunoprecipitation (ChIP) assays revealed increased RelA (p65) binding but decreased c-Jun binding within the *Mir22hg* promoter region upon LPS treatment of BMDCs compared to unstimulated cells (Fig. 3g). MG132 further impaired both *Mir22hg* and miR-22 expression in nCB-treated BMDCs (Fig. 3h,i). Together, these observations indicate that NF-κB enhances *Mir22hg* promoter activity in APCs, suggesting that miR-22 is an NF-κB responsive miRNA in these cells.

To further understand the role of NF-κB and related genes in regulating miR-22 expression, we examined miR-22 abundance in PPAR-γ–deficient lung APCs. We and others previously demonstrated that PPAR-γ is an inhibitor of NF-κB activity and emphysema development[14,15]. Consistent with these observations, miR-22 levels were upregulated in PPAR-γ–deficient lung APCs compared with PPAR-γ–sufficient control APCs (Supplementary Fig. 5a). Moreover, intranasal treatment of smoke-exposed mice with the PPAR-γ agonist ciglitazone reduced miR-22 expression in lung APCs (Supplementary Fig. 5b). Taken together, these observations indicate that PPAR-γ inhibits miR-22 expression in APCs, likely through the inhibition of NF-κB activity. These findings provide insight into the transcriptional mechanism underlying the enhanced miR-22 expression seen in APCs derived from emphysema patients.

Requirement for miR-22 in APC activation

To further determine the immunological importance of miR-22 in APCs, pro-inflammatory molecule mRNA expression profiles were determined in $CD11c^+$ APCs isolated from lungs of wild-type and $Mir22^{-/-}$ mice that were exposed to nCB. As compared to wild-type APCs, $Mir22^{-/-}$ lung APCs expressed less mRNA encoding c-Jun (a subunit of AP-1), the co-stimulatory molecules CD86 and CD40, the chemokine CCL8, and the metalloproteases MMP13 and MMP14 (Fig. 4a, Supplementary Fig. 6). After treatment with LPS or agonistic CD40 antibody overnight, $Mir22^{-/-}$ BMDCs further showed significantly reduced CD86 and CD40 surface expression and secreted less IL-6 (Fig. 4b – d). *In vitro* nCB also induced less IL-6 secretion from $Mir22^{-/-}$ BMDCs as compared to wild-type cells (Fig. 4e). nCB treated miR-22–deficient BMDCs induced less IL-17A from co-cultured naïve wild-type T cells compared to miR-22–sufficient control APCs. However, this defect in IL-17A secretion was abrogated by the addition of IL-6 to the culture conditions (Supplementary Fig. 7). Conversely, transfection of miR-22 mimics into unstimulated mouse BMDCs was

alone sufficient to induce *Il1b*, *Il6*, *Il23a* and *Cd86* mRNA (Fig. 4f) and also enhanced LPS- and agonistic CD40 antibody-dependent IL-6 secretion (Fig. 4g). In a dose-dependent manner, miR-22 was similarly required for robust LPS-dependent IL-6 secretion from human MoDCs (Fig. 4h). Thus, miR-22 drives production of the cytokines such as IL-6 and co-stimulatory molecules that are required for robust T_H17 responses.

Impaired AP-1 activity in *Mir22*$^{-/-}$ APCs

CD40 ligation triggers APC maturation mainly through NF-κB and AP-1, two transcription factors that promote inflammatory cytokine and co-stimulatory molecule expression[16–19]. To determine if miR-22 regulates NF-κB and AP-1 activation in APCs, wild-type and *Mir22*$^{-/-}$ mouse BMDCs were treated with agonistic CD40 antibody. As assessed by immunoblot, no significant difference in the production of p50 and p52 fragments from NF-κB1 (p105) and NF-κB2 (P100) precursors was seen (Fig. 5a). We further determined the phosphorylation status of major signaling proteins in BMDCs from wild-type and *Mir22*$^{-/-}$ mice by reverse phase protein array (RPPA). Phosphorylation of c-Jun increased in wild-type BMDCs after anti-CD40 treatment, but not in *Mir22*$^{-/-}$ BMDCs while phosphorylation of the upstream MAP kinases, MEK1, p38α, Erk1/2 and Jnk showed similar patterns, suggesting that lack of c-Jun phosphorylation in *Mir22*$^{-/-}$ BMDCs was not due to disruption of upstream kinase pathways (Fig. 5b). We next examined the expression of c-Jun in wild-type and *Mir22*$^{-/-}$ BMDCs by immunoblot. Expression of c-Jun increased in wild-type BMDCs after anti-CD40 treatment but decreased in *Mir22*$^{-/-}$ BMDCs. After 24 h of stimulation, there was less c-Jun in *Mir22*$^{-/-}$ relative to wild-type BMDCs, suggesting that miR-22 is an important regulator of c-Jun expression in APCs (Fig. 5c). To address this further, an AP-1 reporter plasmid containing a GFP sequence controlled by an AP-1-specific promoter element was transfected into both wild-type and *Mir22*$^{-/-}$ BMDCs. Wild-type BMDCs generated a significantly stronger GFP signal than *Mir22*$^{-/-}$ BMDCs upon anti-CD40 stimulation (Fig. 5d). Collectively, these data confirm that miR-22 promotes AP-1 transcriptional activity in APCs.

MiR-22 targets histone deacetylase 4 (HDAC4) in APCs

MiR-22 putatively regulates several hundred genes (www.targetscan.org). To begin to determine the critical miR-22-dependent genes that underlie T_H17 responses and emphysema, we again compared gene expression profiles of CD11c$^+$ APCs isolated from wild-type and *Mir22*$^{-/-}$ mouse lungs exposed to nCB, focusing on putative miR-22 target genes that were downregulated in wild-type APCs but less downregulated in *Mir22*$^{-/-}$ APCs (Fig. 6a). To screen for functional relevance to APC activation, we then knocked down the most highly differentially expressed genes (*Ogn*, *Hdac4* and *Acvr2b*) in anti-CD40-activated *Mir22*$^{-/-}$ BMDCs using siRNA. Of these putative targets, the impairment in IL-6 secretion previously shown for *Mir22*$^{-/-}$ BMDCs upon anti-CD40 stimulation was partially restored only by knockdown of HDAC4 (Fig. 6b), which has been previously shown to be a bona fide miR-22 target[20–22]. To confirm that miR-22 regulates HDAC4 expression in APCs, we first showed that neutralization of miR-22 in naïve mouse BMDCs using an antisense locked-nucleic acid (LNA) enhanced both *Hdac4* mRNA and HDAC4 protein (Fig. 6c,d). Moreover, after anti-CD40 stimulation, HDAC4 protein expression decreased in wild-type but increased in *Mir22*$^{-/-}$ BMDCs (Fig. 6e). Finally, knocking down HDAC4 by siRNA

restored the ability of wild-type T cells to secrete IL-17A in the presence of nCB-stimulated *Mir22*$^{-/-}$ or miR-22 LNA transfected BMDCs (Fig. 6f,g). Collectively, these studies confirm that *Hdac4* is a major miR-22 target gene in APCs and suggest the existence of an obligatory regulatory pathway in which activated APCs enhance expression of miR-22 that then inhibits HDAC4 expression to promote T_H17 responses.

HDAC4 inhibits APC activation and emphysema development

HDAC4 is a member of the Class II histone deacetylases and is therefore a potential epigenetic regulator[23,24]. By deacetylating histones in gene promoter regions, chromosomal condensation occurs, reducing the potential of genes in these regions to be transcriptionally activated. Prior studies showed that loss of HDAC4 in myeloid cells results in exacerbated inflammation in high-fat diet-fed mice, suggesting that APC-specific HDAC4 plays an anti-inflammatory role in some contexts[25]. To establish a potential link between HDAC4 and emphysema, we first quantified the expression of *HDAC4* or *Hdac4* mRNA in human MoDCs and mouse BMDCs, respectively, with and without nCB challenge. *HDAC4* (*Hdac4*) mRNA expression was significantly downregulated after nCB challenge of both MoDCs and BMDCs (Fig. 7a,b).

We then created mouse conditional *Hdac4* APC deletants (*Hdac4*^{CD11c}) by crossing mice with a floxed *Hdac4* allele (*Hdac4*^{flox} mice) with mice expressing the Cre enzyme under the control of the *Cd11c* promoter (*Cd11c*-Cre mice). HDAC4-deficient BMDCs generated from *Hdac4*^{CD11c} mice secreted more IL-6 in both naïve and activated states in response to LPS and anti-CD40 stimulation compared to control BMDCs generated from *Hdac4*^{flox} mice (Fig. 7c,d). Upon nCB stimulation, HDAC4-deficient BMDCs and splenic DCs induced even more IL-17A production from co-cultured naive T cells. The hyper-induction of IL-17A from HDAC4-deficient cells was partially or totally offset by adding a neutralizing antibody against IL-6 to the cultures (Fig. 7e,f). HDAC4 was previously shown to suppress c-Jun expression[26,27]. Indeed, we found elevated c-Jun expression in *Hdac4*^{CD11c} BMDCs after anti-CD40 stimulation (Fig. 7g). After nCB exposure, *Hdac4*^{CD11c} mice developed multiple parameters of emphysema compared with *Hdac4*^{flox} mice, including exaggerated alveolar enlargement, airway volume and airway macrophage and neutrophil infiltration (Fig. 7h – k). Together, these observations indicate that HDAC4 is a potent suppressor of nCB-dependent inflammation and that miR-22-dependent HDAC4 suppression is required for full expression of the emphysema phenotype.

Anti-miR-22 treatment reverses mouse emphysema

The preceding studies suggested that either neutralization of miR-22 or enhanced expression of HDAC4 *in vivo* would attenuate development of emphysema. As it is not technically possible to enhance the activity of constitutive HDAC4 *in vivo*, we instead neutralized miR-22 *in vivo* by delivering an anti-miR-22 LNA intranasally to emphysematous mice that were previously exposed to nCB (4 months, Fig. 8). After one month of treatment with a scrambled LNA, mice continued to develop severe emphysema (5 months, Fig. 8). In contrast, mice treated with an anti-miR-22 inhibitory LNA showed evidence of resolving emphysema as determined by CT-based lung volume quantitation and lung histology (5 months, Fig. 8a, b). We continued to treat the two mouse groups similarly for two additional

months and after a total of three months of LNA treatment, control mice showed continued disease progression, whereas the anti-miR-22-treated mice had significantly reduced lung volumes such that they were statistically indistinguishable from control animals (7 months, Fig. 8a). Three months after the cessation of LNA treatments, emphysema returned fully (10 months, Fig. 8a,b).

After one month of anti-miR-22 LNA treatment, miR-22 was essentially undetectable in mouse lungs (Supplementary Fig. 8a). These mice further showed reduced macrophage and neutrophil lung infiltration, fewer T_H17 cells from whole lung, and diminished IL-6 and IL-17A secretion into lung homogenates (Fig. 8c–e; Supplementary Fig. 8b,c). We also found enhanced *Hdac4* mRNA in $CD11c^+$ lung APCs from mice treated with anti-miR-22 LNA and, conversely, reduced *Il6* and *Cd40* transcript expression (Supplementary Fig. 8d – f). Mice previously treated with miR-22 LNA still showed reduced macrophage and neutrophil lung infiltration, but comparable numbers of T_H17 cells from whole lung compared with mice previously treated with scrambled LNA (Fig. 8c – e). Thus, prolonged treatment with anti-miR-22 inhibitory LNA can reverse fully established emphysema and lung APC activation.

Discussion

We have shown that miR-22 is a critical regulator of DC activation in response to cigarette smoke and smoke-derived nCB that is phagocytosed by diverse lung APCs. nCB-activated lung DCs secrete IL-6 and express discrete co-stimulatory molecules that are required for T_H17 cell differentiation and effector function and which we show are controlled through miR-22. Although miR-22 likely influences many immune-related genes, much of the pro-inflammatory activity of miR-22 was mediated through the post-translational suppression of HDAC4. Together, these findings expand our understanding of miRNAs in immunity and reveal a new strategy to treat emphysema and potentially other T_H17-related pathological conditions.

MiR-22 has previously been linked to controlling the cardiac response to acute stress[28,29] and regulating the differentiation of mesenchymal stem cells[30], but to our knowledge this is the first demonstration of a critical immune function for this miRNA. Like many other miRNAs, miR-22 has also been linked to cancer phenotypes. In some contexts, miR-22 is viewed as a tumor suppressor[31], with multiple human tumors showing repression of miR-22 expression in comparison to surrounding normal tissue[32]. In contrast, overexpression of miR-22 induces myelodysplastic syndrome and bone marrow malignancies in mice, suggesting that this microRNA may under other circumstances act as a tumor promoter[33]. Over the approximately 5 years that we have monitored our miR-22-deficient mouse colony, we have yet to notice early mortality or tumors of any kind arising. Moreover, we have not noticed unusual mortality or tumors occurring in wild-type mice treated with anti-miR-22 LNAs. Thus, whereas manipulation of any miRNA or other genetic element carries a theoretical risk of cellular transformation, our experience does not indicate that loss of miR-22 *in vivo* is alone sufficient to promote cancer.

In contrast to miR-22, HDACs have previously been linked to emphysema pathogenesis. HDAC activity from lung biopsies and lung macrophages of smoking patients with emphysema as compared to non-smokers was suppressed in a manner that positively correlated with disease severity[2]. These observations were linked to HDAC2, −5 and −8 and subsequent studies suggested that reduced deacetylation of the glucocorticoid receptor by HDAC2 in emphysema antagonizes the ability of corticosteroids to inhibit the pro-inflammatory potential of NF-κB[9]. Corticosteroids are notoriously ineffective in COPD/emphysema[34], thus this mechanism suggested that interventions that increased activity of HDAC2 might enhance corticosteroid effectiveness. Subsequent study of HDAC inhibitors in rodents and *in vitro* further suggested that HDACs have an anti-inflammatory role in emphysema[35]. However, the broad-spectrum nature of these inhibitors precludes dissection of the most relevant anti-inflammatory HDACs.

Independent lines of evidence have, however, established clear links to immune regulation for HDAC4, which functions as a co-repressor of multiple immune-related transcription factors, including c-Jun, NF-κB and Bcl-6, and regulates IL-5 expresion[26,27,36–38]. HDAC4 also promotes activation of STAT6 and expression of arginase 1 that is required for myeloid DC differentiation[39]. Our studies now show that HDAC4 is essential for suppressing T_H17 responses and nCB-dependent emphysema in mice. Together with our analyses of miR-22, our findings suggest the existence of a pro-inflammatory regulatory loop in which noxious stimuli such as carbon black enhance expression miR-22 that then suppresses HDAC4 sufficiently to promote the differentiation of T_H17-promoting DCs. We have emphasized the role of HDAC4 in controlling DC-derived IL-6, but expression of CD40, CD86 and c-Jun was also impaired in the context of reduced miR-22 and enhanced HDAC4 activity. As all of these factors are required for its development, our findings explain why a pleiotropic suppressive factor such as HDAC4 is required for the regulation of the highly complex T_H17 response[40–43].

Our findings do not rule out a potential role for HDAC2 and other HDACs in the regulation of inflammation in emphysema. Nonetheless, our mechanistic dissection of the pro-inflammatory role of miR-22 in emphysema has revealed that HDAC4 specifically regulates smoking-related lung inflammation and T_H17 responses and may account for much of the HDAC-related anti-inflammatory activity that has previously been reported based on inhibitors. IL-17A and T_H17 cells have also been linked to many chronic diseases other than emphysema that are related to immune dysregulation, including asthma[44], inflammatory bowel disease[45,46], rheumatoid arthritis[47] and others. Interventions that inhibit miR-22 or enhance HDAC4 activity may thus be broadly useful in the therapy of many human diseases caused by chronic inflammation.

Online Methods

Mice

C57BL/6 and B6-Albino (B6(Cg)-*Tyr*$^{c\text{-}2J}$/*J*) were purchased from Jackson Laboratory. *Mir22*$^{-/-}$ (*miR-22*-null) mice used here were generated as previously described[27] and backcrossed at least five generations onto the C57BL/6 background) and then maintained as a homozygous stock. *Hdac4*$^{flox/flox}$ mice were provided by E. Olson (University of Texas

Southwestern Medical Center, Dallas, Texas, USA)[48]. *CD11c*-Cre transgenic mice (8 generations backcrossed to the C57BL/6 background) were provided by J. Levitt at Baylor College of Medicine. For all mouse experiments, wild-type littermate syngeneic animals were used as controls. All mice were bred and maintained in the specific pathogen free Transgenic Mouse Facility at Baylor College of Medicine, fed water and standard rodent chow ad libitum and used in accordance with all federal and institutional guidelines for the humane treatment of animals.

Human subjects

28 non-atopic current or former smokers with significant (>20 pack-years, one pack-year equals to smoking one pack of cigarettes per day each year) history of smoking were recruited into studies from the chest or surgical clinics at Methodist and Michael E. DeBakey Houston Veterans Affairs Medical Center hospitals. Studies were approved by the Institutional Review Board at Baylor College of Medicine, and informed consents were obtained from all patients. Emphysema and non-emphysema control patients were diagnosed according to the criteria recommended by the National Institutes of Health–World Health Organization workshop summary[49].

Dendritic cell preparation from bone marrow

Bone marrow cells isolated from eight-week old mice were lysed of RBC using ACK (Ammonium-Chloride-Potassium) after which cells were washed with complete medium (RPMI 1640 medium, supplemented with 10% Hyclone heat-inactivated FBS, GE Healthcare Life Sciences) and plated in 6-well plates at 5–10 × 10^5 cells/ml. The culture medium was supplemented with mouse GM-CSF (20 ng/ml) and IL-4 (10 ng/ml) (R&D Systems Inc.). On day 5 or 6, both adherent and non-adherent cells were harvested by gently scraping. $CD11c^+$ BMDCs were isolated with bead-conjugated anti-CD11c (Miltenyi) using autoMACS.

Human sample preparation

Human lung single cell suspensions were prepared as previously described[6]. Briefly, fresh lung tissue was cut into 0.1 cm pieces in Petri dishes and treated with 2 mg/ml of collagenase D (Roche Pharmaceuticals) in HBSS for 30 to 40 min at 37 °C. Single cells were collected by mincing and pressing lung tissue through 40 μm cell strainers (BD Biosciences) followed by RBC lysis. Lung DCs were isolated by labeling RBC-free lung cells with CD1a Microbeads (Miltenyi Biotec) and then isolated by AutoMACS separator (Miltenyi). PBMCs were isolated by Ficoll-Paque (GE Healthcare) density gradient centrifugation. Human MDDCs were prepared as previously described. Briefly, RBC-free PBMCs were seeded in 6-well plates for two hours at 37°C and then non-adherent cells were removed by washing with PBS. Adherent cells were cultured with 50 ng/ml recombinant human GM-CSF and 10 ng/ml recombinant human IL-4 (R&D Systems Inc.) for 5 or 6 days. Both adherent and non-adherent cells were collected by gently scraping for further assays.

Immune cell isolation

Mouse lung and spleen single-cell suspensions were prepared and RBC were lysed using ACK buffer as previously described[50]. RBC-free lung cells were washed with complete medium and labeled with bead-conjugated anti-CD11c (Miltenyi) to isolate lung APCs using autoMACS. RBC-free splenic cells were labeled with bead-conjugated anti-CD4 (Miltenyi) to isolate $CD4^+$ T cells.

MiR-22 neutralization in vivo

An antisense miR-22 locked nucleotide acid (LNA), 5′-CTTCAACTGGCAGCT-3′, and scrambled control LNA, 5′-ACGTCTATACGCCCA-3′, were synthesized by Exiqon. The LNAs were first reconstituted into ultra-pure water (Invitrogen) and further diluted to working stock (0.4 mg/ml) by sterile PBS. 50 μl working stock LNA was intranasally delivered into mouse lung three times a week for four weeks.

Cigarette smoke exposure model of pulmonary emphysema

Mice were exposed to cigarette smoke as previously described[8]. Eight-week old mice were exposed to four commercial cigarettes (Marlboro 100's; Philip Morris USA) per day, five days a week, for four months. One week after last cigarette smoke exposure, lung volumes were determined by microCT imaging as described previously[8]. Mice were anesthetized with etomidate (30 mg per kg body weight) and scanned in an animal CT scanner (Gamma Medica) in the Animal Phenotyping Core at Baylor College of Medicine. Three-dimensional models of mouse lung were reconstructed and the volume were calculated by Amira 3.1.1 software. Bronchoalveolar lavage fluid (BALF) cell differential counting, lung tissue collection and lung histopathology were performed as previously described[51]. Briefly, mice were anesthetized with etomidate, BALF was collected by instilling and withdrawing 1 ml of sterile PBS twice through the tracheal cannula. Mouse lungs were either dissected to prepare single cell suspensions or fixed with 4% paraformaldehyde solution for histopathological studies. $CD11c^+$ lung antigen presenting cells were labeled by CD11c MicroBeads (Miltenyi) and isolated from lung single cell suspensions by AutoMACS Separator (Miltenyi).

Carbon black nanoparticle exposure model of pulmonary emphysema

Commercial grade CB (Cabot Corporation; 15 nm, lot 1278105) composed of 15 nm particles in clusters of 3–5 particles were suspended in *tert*-Butyl alcohol with 1% sucrose, the latter added to prevent aggregation in aqueous suspension, and then lyophilized at −80 °C overnight. Dried nCB nanoparticles were resuspended in sterile PBS to a concentration of 10 mg/ml. 50 μl reconstituted nCB (0.5 mg) were intranasally delivered to deeply anesthetized mice on a schedule of three times a week for six weeks (total delivered dose of 9 mg). Lung volume and airway inflammation were assessed four weeks after the final nCB challenge.

APC–T cell co-culture

Isolated human or mouse $CD4^+$ T cells were co-cultured with APCs at a ratio of 10:1 in 96-well U bottom tissue culture plates with complete medium supplemented with anti-CD3ε

antibody (clone: 145-2C11, 1 μg/ml, BD Bioscience). The medium and cells were collected on day 3 for further analysis.

ELISA and Bioplex system

Mouse and human IL-1β, IL-6 and TNF were measured by BD OptEIA ELISA kits (BD Bioscience) according to manufacturer's guidelines. Mouse IL-4, IFN-γ, IL-17A and human IL-17A were measured by sandwich ELISA with antibody pairs from R&D system. Other human and mouse cytokines and chemokines were measured by Milliplex Assays (EMD Millipore) performed on the Bioplex 100 system (Bio-Rad Loboratories).

RNA isolation and quantitative PCR

Fresh cell pellets were collected and stored in TRIZOL (Invitrogen). Total RNA was extracted with chloroform (Sigma-Aldrich), and precipitated in isopropanol (Sigma-Aldrich). The concentration of total RNA was determined NanoDrop 2000 (Thermo Fisher Scientific) and the cDNA of total messenger RNA or microRNA were synthesized by High-Capacity cDNA Reverse Transcription Kit or TaqMan® MicroRNA Reverse Transcription Kits (Life Technologies), respectively, according to manufacturer's guidelines. Quantitative PCR was performed using the ABI Perkin Elmer Prism 7500 Sequence Detection System (Applied Biosystems) using standard protocols. All Taqman probes were from Applied Biosystems.

Quantitative Flow cytometry

Flow cytometry was performed with BD LSRII or Accuri C6 (BD Biosciences) and analyzed with Flowjo software (www.flowjo.com). To quantify the absolute number of specific cell types residing in samples, Flow-Set Fluorospheres beads (Beckman Coulter Inc) were mixed into all samples beforehand as input controls. Event numbers of all cell populations were normalized to the number of fluorospheres beads to generate the absolute number.

Antibodies and other reagents

Mouse specific antibodies: Pacific Blue-CD3 (500A2), APC-Cy7-CD8 (53-6.7), PE-IL17A (TC11-18H10), APC-IFN-γ (XMG1.2), PE-Cy5-CD4 (PM4-5), were purchased from BD Pharmingen. FITC-γδTCR (eBioGL3), eFluro450-B220 (RA3-6B2), PE-CD11b (M1/70), APC-CD11c (N418) were purchased from eBioscience.

Lung APC gene expression

Mouse $CD11c^+$ lung APC gene expression profiling was performed using the Illumina MouseWG-6 v2 Expression BeadChip Array (Expression Analysis, Inc). Probes with signal less than 20 units were pre-filtered. Data were analyzed with variance-stabilizing transform and quantile normalization. The heatmaps were generated in Cluster 3.0 (http://bonsai.hgc.jp/~mdehoon/software/cluster/software.htm) as a hierarchical cluster using Pearson correlation and a centered metric. The resulting heatmap was visualized and presented by Treeview (http://www.eisenlab.org/eisen).

Chromatin immunoprecipitation (ChIP) assay

ChIP experiments were performed using the Pierce Agarose ChIP Kit (Thermo Fisher Scientific) according to the manufacturer's protocols. In brief, for each analysis, 4×10^6 differentially treated mouse BMDCs were cross-linked with 1% formaldehyde at 24°C for 10 min followed by adding 0.2 M glycine for 5 min at 24°C. Chromatin was digested with micrococcal nuclease and immunoprecipitated with ChIP grade p65, Jun, acetyl-histone H3 antibody or rabbit IgG (Cell Signaling Technology) together with agarose beads overnight at 4 °C. DNA was thereafter recovered using a DNA column. *Mir22hg* promoter region was amplified by PCR (forward primer, 5′-GCGACCGAGTCAGAGATCAG-3′; reverse primer, 5′-CCTCTGCTTACTCCCGCCC-3′).

Reverse phase protein array (RPPA)

Mouse BMDCs were activated in the presence of agonistic CD40 antibody (R&D systems, clone: 1C10) and collected by gentle scraping followed by snap freezing in liquid nitrogen. All samples were analyzed in the RPPA Core Facility at MD Anderson Cancer Center (Houston, Texas, USA) and processed according standard procedures. Briefly, serially diluted cellular lysates were denatured with 1% SDS and beta-mercaptoethanol before loading onto nitrocellulose-coated array slides (Grace Biolab) by 2470 Arrayer (Aushon BioSystems). Each slide was probed with primary antibodies plus biotin-conjugated secondary antibodies. Probed array slides were scanned, analyzed and quantified using Microvigene (VigeneTech Inc.). Each dilution curve was fitted with a standard fitting curve and normalized with a loading correction factor to generate expression levels of all analytes for each sample. The heatmaps of LOG2 transformed antibody expression level data were generated in Cluster 3.0 (http://bonsai.hgc.jp/~mdehoon/software/cluster/software.htm) as a hierarchical cluster using Pearson correlation and a centered metric. The resulting heatmap was visualized and presented by Treeview (http://www.eisenlab.org/eisen).

Gelatin gel zymography

MMP2 and MMP9 proteinase activity in BALF was quantified by Zymography as previously described[52]. Briefly, 15 μl BAL fluid was initially separated in 10% SDS-polyacrylamide gels with 2% gelatin. SDS was removed from gels using 2.5% Triton X-100 immediately after electrophoresis. SDS-free gels were incubated in developing buffer (50 mM Tris-HCl at pH 8, 5 mM $CaCl_2$, and 0.02% NaN_3) overnight at 37 °C. Gels were then fixed and stained with coomassie blue. MMP2 and MMP9 appear as transparent bands on blue background around 70 kDa and 100 kDa range, respectively.

OVA sensitization

Mice were intraperitoneally sensitized with OVA precipitated in alum once a week for three continuous weeks as previously described[50]. T helper cell subsets were quantified from splenocytes by the end of the fourth week.

Statistics

Data are presented with 3–7 mice/group for *in vivo* experiments and a minimum of 4 replicates/condition for *in vitro* experiments. Significant differences for paired groups were

determined using the Mann-Whitney test and for multiple comparisons using the Kruskal-Wallis test.

Supplementary Material

Refer to Web version on PubMed Central for supplementary material.

ACKNOWLEDGMENTS

Supported by the US National Institutes of Health (R01HL117181 to F. K., R01HL110883 to F. K. and D.B.C., and AI036211, CA125123, and RR024574 to the Cytometry and Cell Sorting Core at Baylor College of Medicine), and the US Veterans Administration Office of Research and Development (1I01BX002221 to D.B.C.). We thank J. Levitt (Baylor College of Medicine) for providing the *CD11c–Cre* mice; E. Olson (UT Southwestern Medical Center) for providing the *Hdac4*^{flox} mice; and W. Decker, J. Sederstrom, Y. Qian and L.-Z. Song for technical assistance.

References

1. Hoyert DL, Xu JQ. Deaths: preliminary data for 2011. Natl. Vital Stat. Rep. 2012; 61:1–65. [PubMed: 24984457]
2. Wilson DO, et al. Association of radiographic emphysema and airflow obstruction with lung cancer. Am. J. Respir. Crit. Care Med. 2008; 178:738–744. [PubMed: 18565949]
3. Hart JE, Eisen EA, Laden F. Occupational diesel exhaust exposure as a risk factor for chronic obstructive pulmonary disease. Curr. Opin. Pulm. Med. 2012; 18:151–154. [PubMed: 22234274]
4. Xu C, et al. Autoreactive T Cells in Human Smokers Is Predictive of Clinical Outcome. Front. Immunol. 2012; 3:267. [PubMed: 22969766]
5. Grumelli S, et al. An immune basis for lung parenchymal destruction in chronic obstructive pulmonary disease and emphysema. PLoS Med. 2004; 1:75–83.
6. Shan M, et al. Lung myeloid dendritic cells coordinately induce TH1 and TH17 responses in human emphysema. Sci. Transl. Med. 2009; 1:28.
7. Shan M, et al. Agonistic induction of PPAR-γ reverses cigarette smoke induced emphysema. J. Clin. Invest. 2014; 124:1371–1381. [PubMed: 24569375]
8. Shan M, et al. Cigarette smoke induction of osteopontin (SPP1) mediates T(H)17 inflammation in human and experimental emphysema. Sci. Transl. Med. 2012; 4:18.
9. O'Connell RM, Rao DS, Chaudhuri AA, Baltimore D. Physiological and pathological roles for microRNAs in the immune system. Nat. Rev. Immunol. 2010; 10:111–122. [PubMed: 20098459]
10. Polikepahad S, et al. Proinflammatory role for let-7 microRNAS in experimental asthma. J. Biol. Chem. 2010; 285:30139–30149. [PubMed: 20630862]
11. You R, et al. Nanoparticulate Carbon Black in Cigarette Smoke Induce DNA Cleavage and Th17-Mediated Emphysema. eLife. (Submitted).
12. Rincon M, Irvin CG. Role of IL-6 in asthma and other inflammatory pulmonary diseases. Int. J. Biol. Sci. 2012; 8:1281–1290. [PubMed: 23136556]
13. Rodriguez A, Griffiths-Jones S, Ashurst JL, Bradley A. Identification of mammalian microRNA host genes and transcription units. Genome Res. 2004; 14:1902–1910. [PubMed: 15364901]
14. Hou Y, Moreau F, Chadee K. PPARgamma is an E3 ligase that induces the degradation of NF-κB/p65. Nat Commun. 2012; 3:1300. [PubMed: 23250430]
15. Shan M, et al. Agonistic induction of PPARgamma reverses cigarette smoke-induced emphysema. J. Clin. Invest. 2014; 124:1371–1381. [PubMed: 24569375]
16. Greenlee KJ, Werb Z, Kheradmand F. Matrix metalloproteinases in lung: multiple, multifarious, and multifaceted. Physiol. Rev. 2007; 87:69–98. [PubMed: 17237343]
17. O'Sullivan BJ, Thomas R. CD40 ligation conditions dendritic cell antigen-presenting function through sustained activation of NF-kappaB. J. Immunol. 2002; 168:5491–5498. [PubMed: 12023343]

18. Mann J, Oakley F, Johnson PW, Mann DA. CD40 induces interleukin-6 gene transcription in dendritic cells: regulation by TRAF2, AP-1, NF-kappa B, AND CBF1. J. Biol. Chem. 2002; 277:17125–17138. [PubMed: 11886848]
19. Oeckinghaus A, Hayden MS, Ghosh S. Crosstalk in NF-κB signaling pathways. Nat. Immunol. 2011; 12:695–708. [PubMed: 21772278]
20. Huang ZP, et al. MicroRNA-22 regulates cardiac hypertrophy and remodeling in response to stress. Circ Res. 2013; 112:1234–1243. [PubMed: 23524588]
21. Jovicic A, Zaldivar Jolissaint JF, Moser R, Silva Santos Mde F, Luthi-Carter R. MicroRNA-22 (miR-22) overexpression is neuroprotective via general anti-apoptotic effects and may also target specific Huntington's disease-related mechanisms. PLoS ONE. 2013; 8
22. Zhang J, et al. microRNA-22, downregulated in hepatocellular carcinoma and correlated with prognosis, suppresses cell proliferation and tumourigenicity. Br. J. Cancer. 2010; 103:1215–1220. [PubMed: 20842113]
23. de Ruijter AJ, van Gennip AH, Caron HN, Kemp S, van Kuilenburg AB. Histone deacetylases (HDACs): characterization of the classical HDAC family. Biochem. J. 2003; 370:737–749. [PubMed: 12429021]
24. Parra M. Class IIa HDACs - new insights into their functions in physiology and pathology. FEBS J. 2014 Oct 27.
25. Luan B, et al. Leptin-mediated increases in catecholamine signaling reduce adipose tissue inflammation via activation of macrophage HDAC4. Cell Metab. 2014; 19:1058–1065. [PubMed: 24768298]
26. Gordon JW, et al. Protein kinase A-regulated assembly of a MEF2-HDAC4 repressor complex controls c-Jun expression in vascular smooth muscle cells. J. Biol. Chem. 2009; 284:19027–19042. [PubMed: 19389706]
27. Wang AH, et al. HDAC4, a human histone deacetylase related to yeast HDA1, is a transcriptional corepressor. Mol. Cell. Biol. 1999; 19:7816–7827. [PubMed: 10523670]
28. Gurha P, et al. Targeted deletion of microRNA-22 promotes stress-induced cardiac dilation and contractile dysfunction. Circulation. 2012; 125:2751–2761. [PubMed: 22570371]
29. Gurha P, et al. microRNA-22 promotes heart failure through coordinate suppression of PPAR/ERR-nuclear hormone receptor transcription. PLoS ONE. 2013; 8
30. Huang S, et al. Upregulation of miR-22 promotes osteogenic differentiation and inhibits adipogenic differentiation of human adipose tissue-derived mesenchymal stem cells by repressing HDAC6 protein expression. Stem Cells & Dev. 2012; 21:2531–2540.
31. Tang Y, et al. microRNA-22 acts as a metastasis suppressor by targeting metadherin in gastric cancer. Mol. Med. Rep. 2015; 11:454–460. [PubMed: 25323629]
32. Xu QF, et al. MiR-22 is frequently downregulated in medulloblastomas and inhibits cell proliferation via the novel target PAPST1. Brain Pathol. 2014; 24:568–583. [PubMed: 24576181]
33. Song SJ, et al. The oncogenic microRNA miR-22 targets the TET2 tumor suppressor to promote hematopoietic stem cell self-renewal and transformation. Cell Stem Cell. 2013; 13:87–101. [PubMed: 23827711]
34. Keatings VM, Jatakanon A, Worsdell YM, Barnes PJ. Effects of inhaled and oral glucocorticoids on inflammatory indices in asthma and COPD. Am. J. Respir. Crit. Care Med. 1997; 155:542–548. [PubMed: 9032192]
35. Mizuno S, et al. Inhibition of histone deacetylase causes emphysema. Am. J. Physiol. Lung Cell Mol. Physiol. 2011; 300(3):L402–L413. [PubMed: 21224215]
36. Lemercier C, et al. Class II histone deacetylases are directly recruited by BCL6 transcriptional repressor. J. Biol. Chem. 2002; 277:22045–22052. [PubMed: 11929873]
37. Sandhu SK, et al. miR-155 targets histone deacetylase 4 (HDAC4) and impairs transcriptional activity of B-cell lymphoma 6 (BCL6) in the Emu-miR-155 transgenic mouse model. Proc. Natl. Acad. Sci. USA. 2012; 109:20047–20052. [PubMed: 23169640]
38. Han S, et al. Recruitment of histone deacetylase 4 by transcription factors represses interleukin-5 transcription. Biochem. J. 2006; 400:439–448. [PubMed: 16922677]

39. Yang Q, et al. Cross Talk between Histone Deacetylase 4 and STAT6 in the Transcriptional Regulation of Arginase 1 during Mouse Dendritic Cell Differentiation. Mol. Cell. Biol. 2015; 35:63–75. [PubMed: 25332236]
40. Liu W, et al. AP-1 activated by toll-like receptors regulates expression of IL-23 p19. J. Biol. Chem. 2009; 284:24006–24016. [PubMed: 19592489]
41. Wang X, et al. Early secreted antigenic target of 6-kDa protein of Mycobacterium tuberculosis primes dendritic cells to stimulate Th17 and inhibit Th1 immune responses. J. Immunol. 2012; 189:3092–3103. [PubMed: 22904313]
42. Bettelli E, et al. Reciprocal developmental pathways for the generation of pathogenic effector T_H17 and regulatory T cells. Nature. 2006; 441:235–238. [PubMed: 16648838]
43. Ivanov II, et al. The orphan nuclear receptor RORgammat directs the differentiation program of proinflammatory IL-17+ T helper cells. Cell. 2006; 126:1121–1133. [PubMed: 16990136]
44. Kudo M, et al. IL-17A produced by αβ T cells drives airway hyper-responsiveness in mice and enhances mouse and human airway smooth muscle contraction. Nat. Med. 2012; 18:547–554. [PubMed: 22388091]
45. Rohn TA, et al. Vaccination against IL-17 suppresses autoimmune arthritis and encephalomyelitis. Eur. J. Immunol. 2006; 36:2857–2867. [PubMed: 17048275]
46. Elson CO, et al. Monoclonal anti-interleukin 23 reverses active colitis in a T cell-mediated model in mice. Gastroenterology. 2007; 132:2359–2370. [PubMed: 17570211]
47. Hirota K, et al. T cell self-reactivity forms a cytokine milieu for spontaneous development of IL-17+ Th cells that cause autoimmune arthritis. J. Exp. Med. 2007; 204:41–47. [PubMed: 17227914]
48. Majdzadeh N, et al. HDAC4 inhibits cell-cycle progression and protects neurons from cell death. Dev. Neurobiol. 2008; 204:1076–1092. [PubMed: 18498087]
49. Pauwels RA, et al. Global strategy for the diagnosis, management, and prevention of chronic obstructive pulmonary disease. NHLBI/WHO Global Initiative for Chronic Obstructive Lung Disease (GOLD) Workshop summary. Am. J. Respir. Crit. Care Med. 2001; 163:1256–1276. [PubMed: 11316667]
50. Corry DB, et al. Interleukin 4, but not interleukin 5 or eosinophils, is required in a murine model of acute airway hyperreactivity. J. Exp. Med. 1996; 183:109–117. [PubMed: 8551213]
51. Lee SH, et al. Differential requirement for CD18 in T-helper effector homing. Nat. Med. 2003; 9:1281–1286. [PubMed: 14502280]
52. Corry DB, et al. Decreased allergic lung inflammatory cell egression and increased susceptibility to asphyxiation in MMP2-deficiency. Nat. Immunol. 2002; 3:347–353. [PubMed: 11887181]

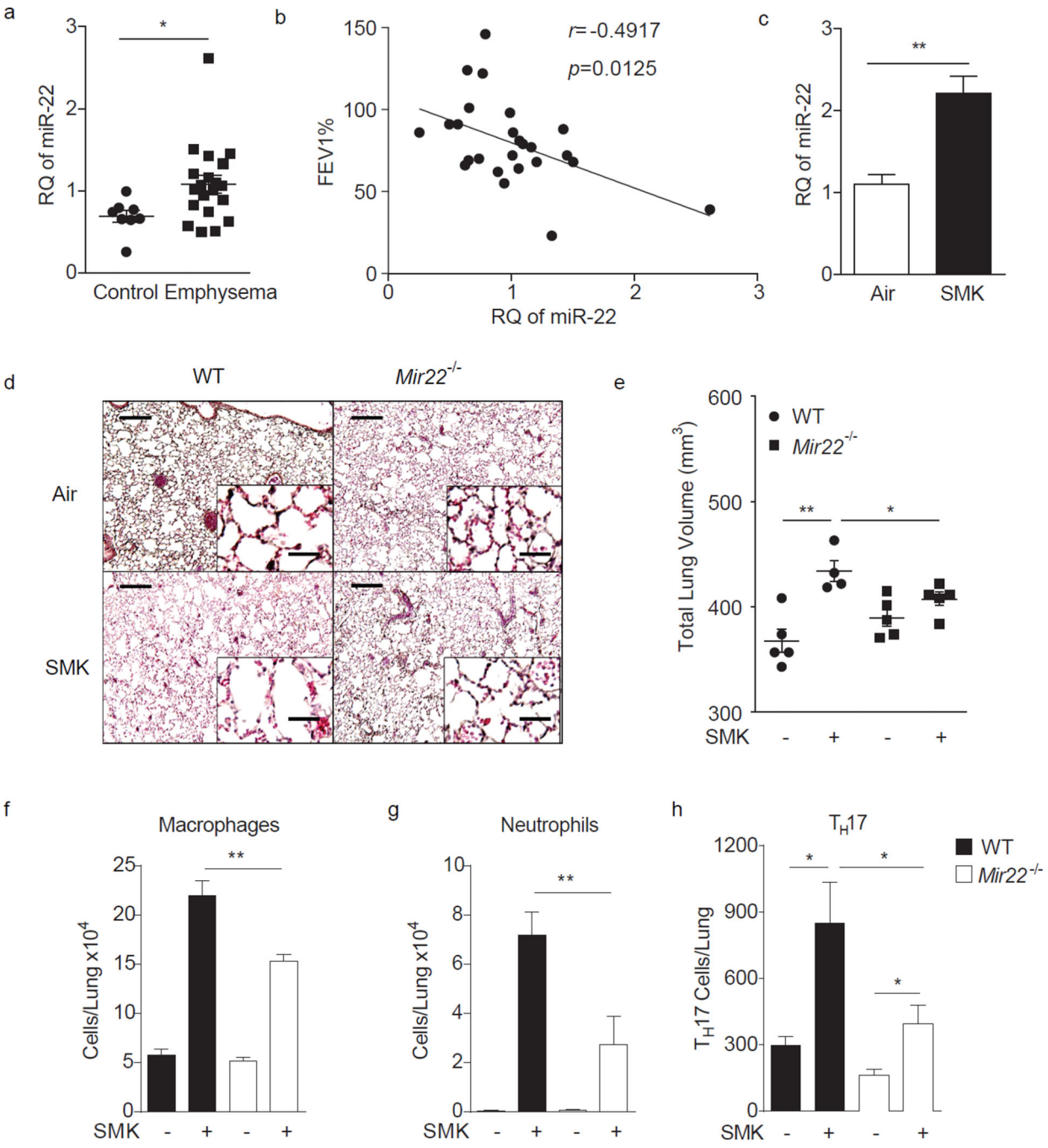

Figure 1.

Enhanced miR-22 expression in human emphysema and cigarette smoke-activated lung APCs. (**a**) Expression of miR-22 in lung CD1a^{+} mDCs from control (*n*=8) and emphysema patients (*n*=20) as determined by RT-qPCR (RQ: relative quantity relative to U6 snRNA). (**b**) Correlation of human miR-22 expression with percent predicted forced expiratory volume in one second (FEV1). (*n*=25) (**c**) MiR-22 expression in lung CD11c^{+} cells from mice exposed to cigarette smoke for 4 months. (*n*=3, represent two independent experiments) (**d–h**) Wild-type (WT) and *Mir22*$^{-/-}$ mice were exposed to air or cigarette

smoke (SMK) for 4 months. (**d**) Representative H&E stained lung sections (of 4 total, 50× magnification; insets: 400×; scale bars: 200 μm; insets: 25 μm). (**e**) Micro-CT quantification of lung volume. Total macrophages (**f**) and neutrophils (**g**) from BALF and total lung IL-17A$^+$ T_H17 cells (**h**) as assessed by flow cytometry. (d–h) *n*=4–5 mice/group as indicated in (e). Data represent one of four comparable experiments. *: $p<0.05$; **: $p<0.01$, (a) Mann Whitney test, (c) unpaired t-test, (e–h) Kruskal Wallis test.

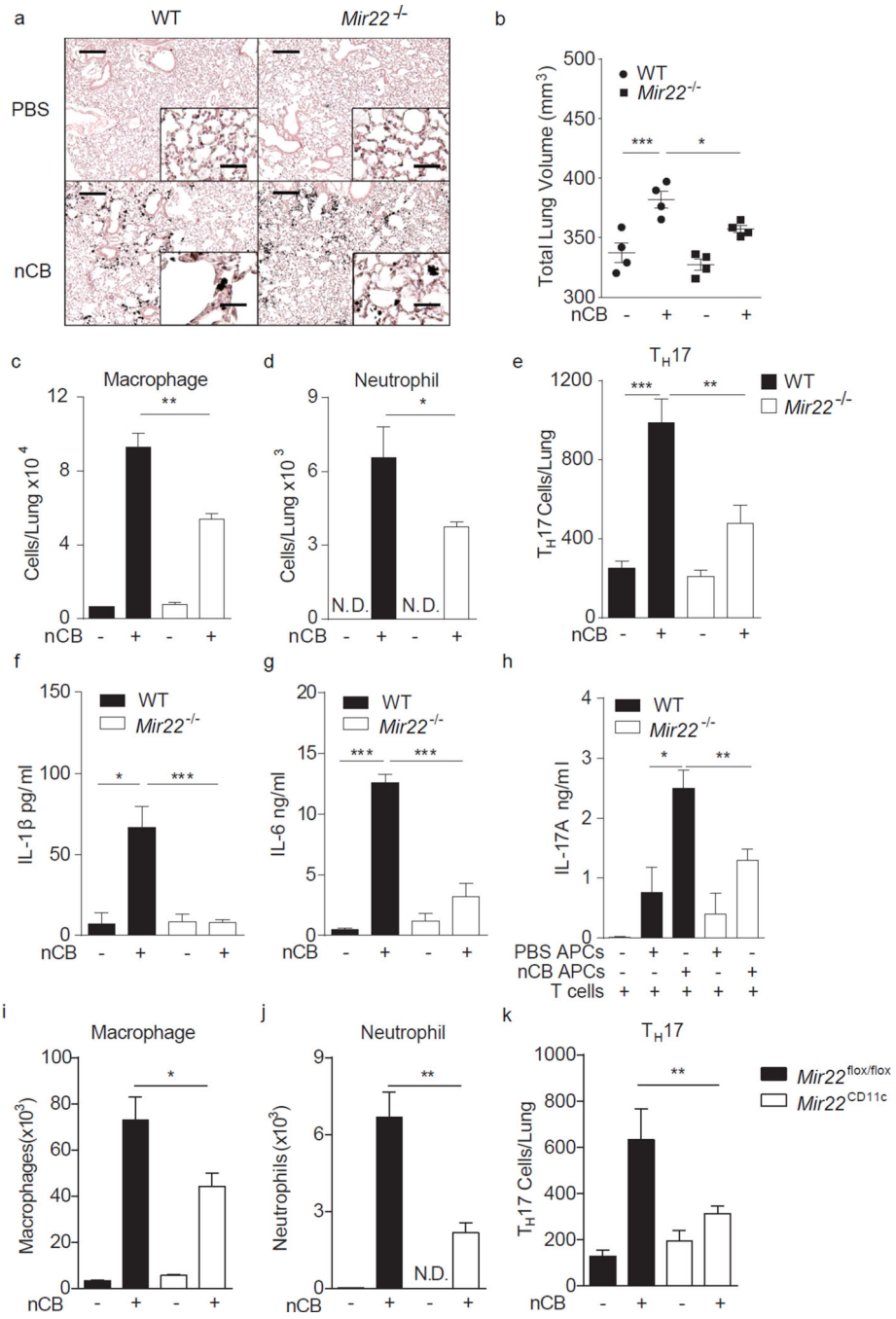

Figure 2.

MiR-22 deficiency protects against nCB-induced emphysema in mice. WT and *Mir22*$^{-/-}$ mice were exposed to vehicle (PBS) or nCB for one month. (**a**) Representative H&E stained lung sections (of 4 total, 50× magnification; insets: 400×; scale bars: 200 μm; insets: 25 μm). (**b**) Micro-CT quantification of lung volume. Macrophages (**c**) and neutrophils (**d**) were quantified from BALF and total lung IL-17A^{+} T_H17 cell (**e**) were assessed by flow cytometry. N.D.: not detected. Lung CD11c^{+} cells were isolated and cultured *ex vivo* overnight and supernatants assayed for secreted IL-1β (**f**) and IL-6 (**g**) by ELISA. (**h**) Lung

$CD11c^+$ APCs isolated from nCB or PBS exposed mice were co-cultured with naïve syngeneic $CD4^+$ T cells *ex vivo* for 3 days and secreted IL-17A was measured by ELISA. (**i–k**) Mice lacking miR-22 in $CD11c^+$ APC ($Mir22^{CD11c}$) and control mice ($Mir22^{flox/flox}$) were exposed to PBS or nCB for one month after which macrophages (**i**) and neutrophils (**j**) were quantified from BALF and total IL-$17A^+$ T_H17 cells (**k**) were enumerated from whole lung. *: $p<0.05$; **: $p<0.01$; ***: $p<0.001$ Kruskal Wallis test; n=4 or as indicated. Data are from one of three comparable experiments.

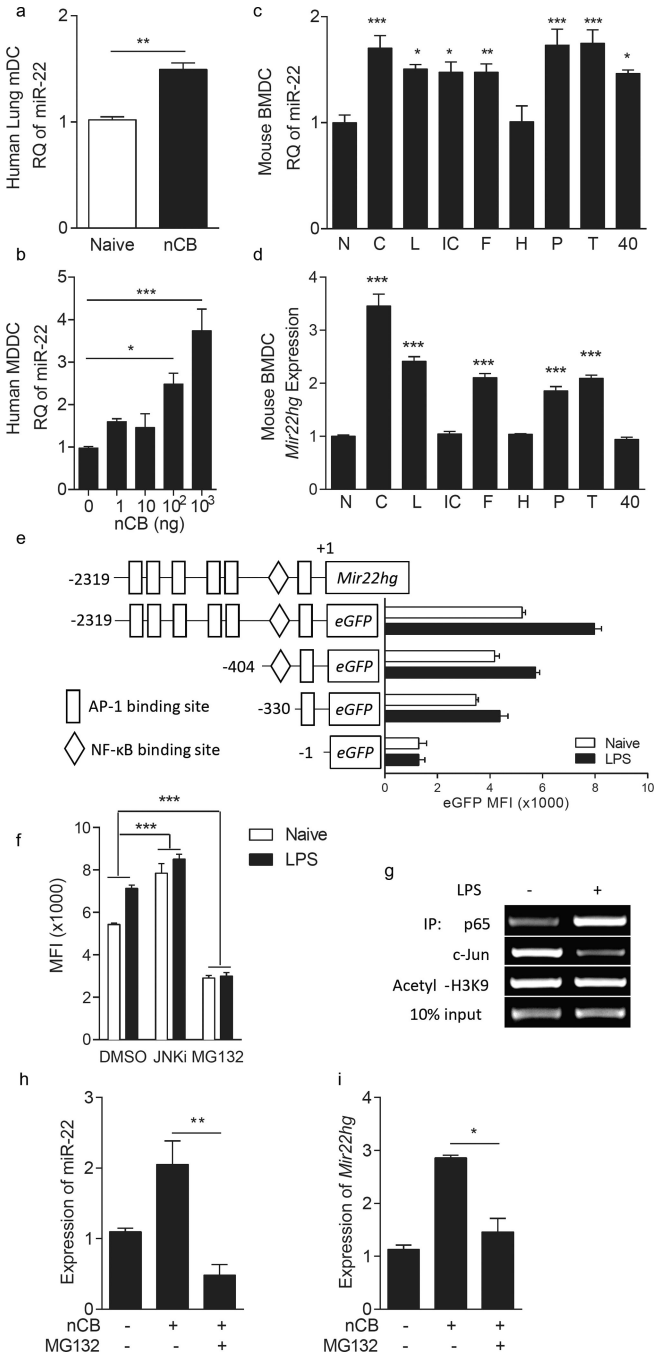

Figure 3.

MiR-22 expression is transcriptionally regulated through NF-κB and AP-1 complexes. (**a,b**) MiR-22 expression in human lung CD1a^{+} cells (**a**) and naïve monocyte derived dendritic cells (**b**) after 2 days of *in vitro* challenge with nCB (nCB; 10^4 ng or as indicated; n=4). (**c,d**) MiR-22 (**c**) and *Mir22hg* (**d**) expression in naïve (N) mouse bone marrow derived dendritic cells or after stimulation with 10^4 ng carbon black (C), 1ng/ml LPS (L), 100ng/ml Poly I:C (IC), 100ng/ml FSL-1 (F), 10^8 cells/ml heat killed *Listeria monocytogenes* (H), 100ng/ml Pam3CSK4 (P), 1μg/ml lipoteichoic acid (T), and agonistic αCD40 antibody (40) overnight

(n=4). RQ: relative quantity to U6 snRNA (**a–c**) or 18S (**d**). (**e**) Schematic representation of the proximal 2.3kb of the *Mir22hg* promoter, including indicated transcription factor binding sites (top) and eGFP reporter constructs (pcDNA3-eGFP) containing the full-length promoter and additional truncation variants. Reporter plasmids were transfected into RAW264.7 cells and eGFP expression with and without LPS stimulation was quantitated by flow cytometry (n=4). (**f**) EGFP expression driven by the 2.3kb promoter in (**e**) in the presence of the NK-κB inhibitor MG132, Jnk inhibitor (JnkI; SP600125) or DMSO vehicle. (**g**) RelA (p65) and Jun binding to the *Mir22hg* promoter in naïve and LPS-stimulated mouse BMDCs as assessed by chromatin immunoprecipitation. (**h,i**) MiR-22 (**h**) and *Mir22hg* (**i**) expression in naïve or nCB treated mouse BMDCs with or without MG132. *, $p<0.05$; **, $p<0.01$; ***, $p<0.001$, Mann-Whitney test in (**a**). (**f**) two-way ANOVA n=3; (**b–d,h,i**) Kruskal Wallis test n=4–5. Data are from one of at least two comparable experiments.

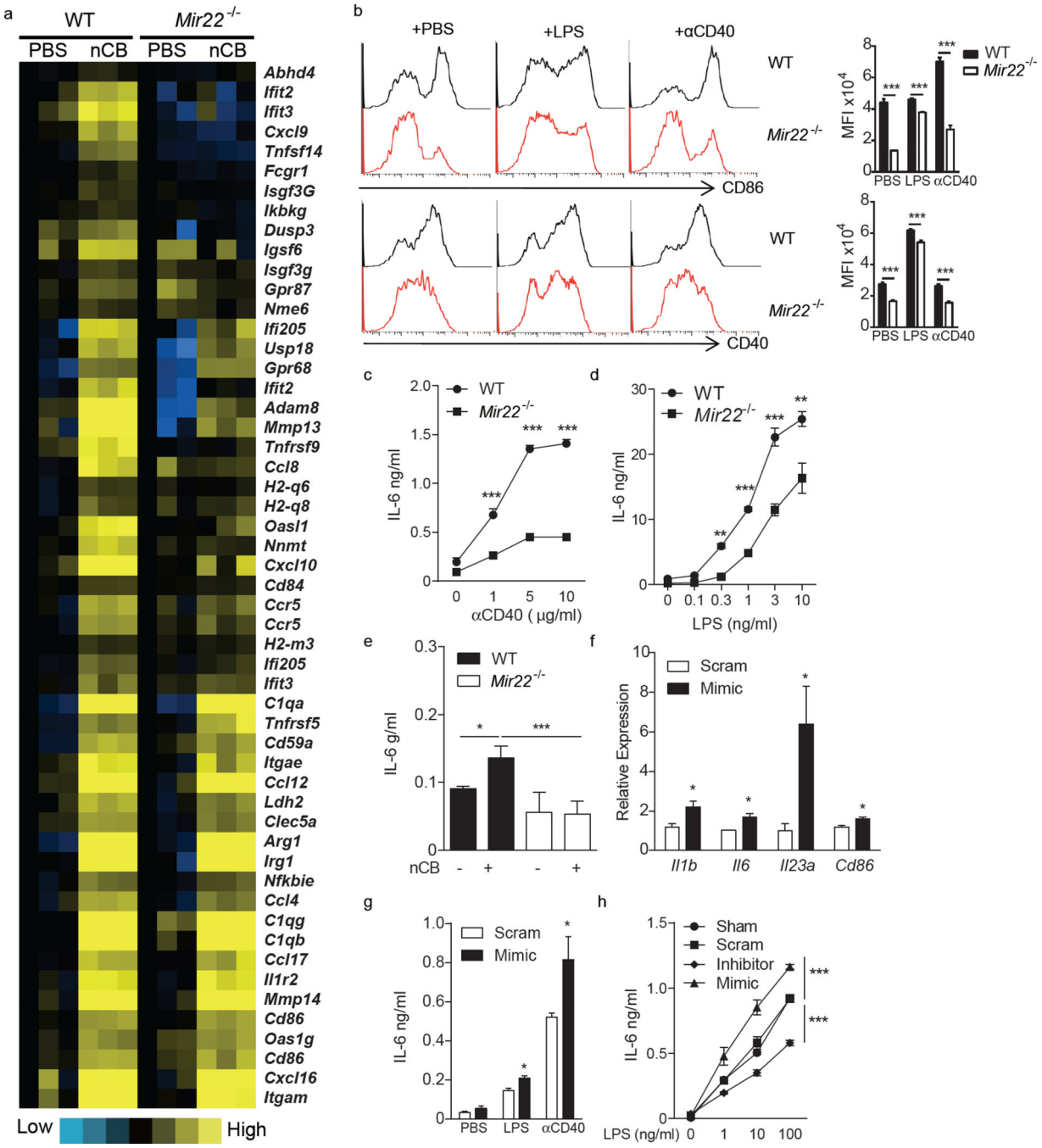

Figure 4.

MiR-22 promotes lung APC activation. Lung CD11c^{+} cells from WT and *Mir22*$^{-/-}$ mice exposed to PBS or carbon black (nCB) were isolated and genome-wide gene expression profiles were determined by illumina gene microarray. (**a**) Heatmap showing selected genes upregulated in WT but less upregulated in *Mir22*$^{-/-}$ mice after nCB exposure. (**b**) CD40 and CD86 expression on WT and *Mir22*$^{-/-}$ BMDCs treated with PBS (N), 1ng/ml LPS (L) or 5μg/ml anti-CD40 agonistic antibody (40). Left panel: single channel histograms showing CD40 and CD86 expression as determined by flow cytometry. Right panel: aggregate mean

fluorescence intensity (MFI) data (n=5). (**c–e**) IL-6 production from WT and *Mir22*$^{-/-}$ BMDCs after increasing doses of αCD40 (**c**), LPS (**d**) or 100ng carbon black (**e**) stimulation (n=5). (**f,g**) WT BMDCs were transfected with scrambled (Scram) or miR-22 mimic (Mimic). (**f**) Expression of the indicated mRNAs was determined by RT-qPCR (n=3). (**g**) IL-6 secretion after PBS, 1ng/ml LPS or 5μg/ml αCD40 stimulation was measured by ELISA (n=4). (**h**) Human monocyte derived dendritic cells were transfected with scrambled (Scram) or miR-22 antisense LNA (LNA), miR-22 mimic (Mimic) or sham-transfected (Sham). IL-6 secretion after stimulation with the indicated amounts of LPS was then measured by ELISA (n=4). *: $p<0.05$; **: $p<0.01$; ***: $p<0.001$, Mann Whitney (**b–d**), unpaired t-test (**f,g**) and Kruskal Wallis tests (**e,h**). Data (**b,h**) are from one of at least two comparable experiments.

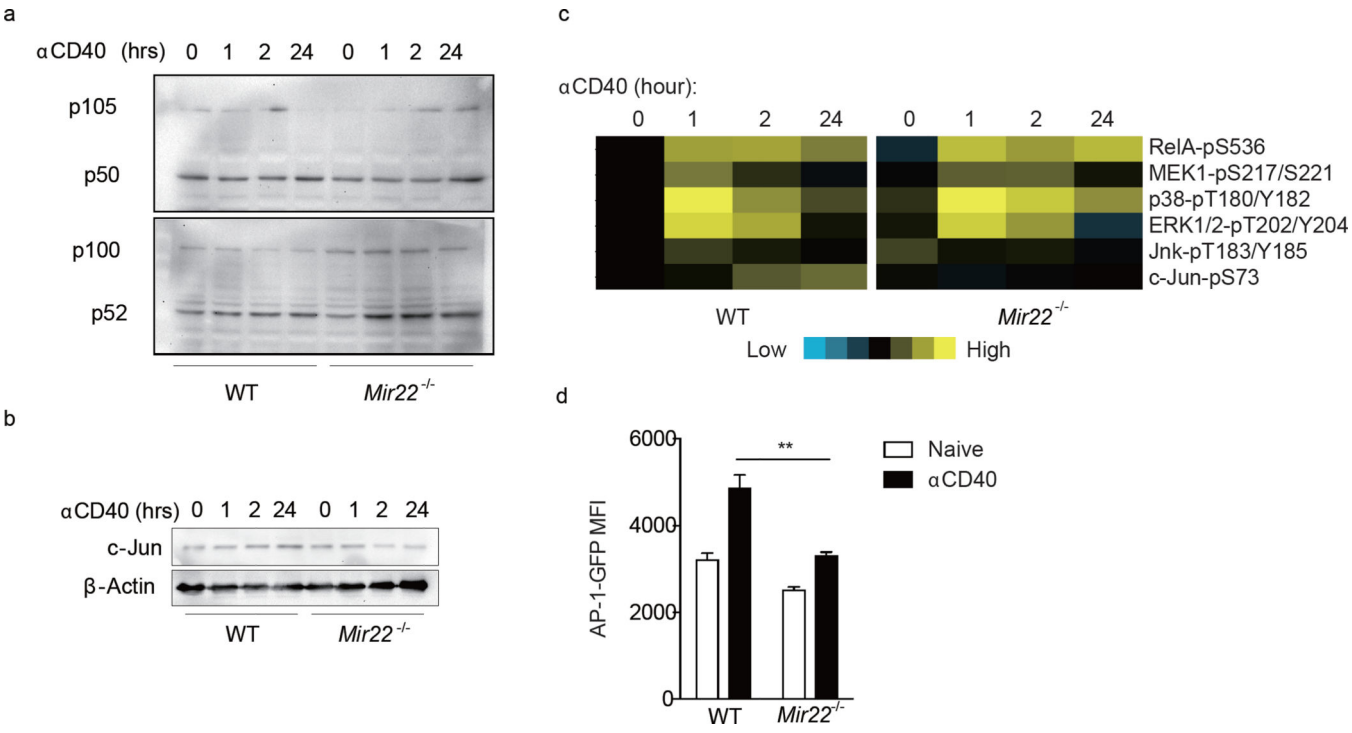

Figure 5.

MiR-22 promotes AP-1 transcriptional activity in APC. WT and *Mir22*$^{-/-}$ BMDCs were stimulated with agonistic CD40 antibody (αCD40) for 1, 2, and 24 hours *in vitro*. Expression of (**a**) NF-κB1 (P105/P50), NF-κB2 (P100/P52) and (**b**) c-Jun was determined by immunoblot. (**c**) Heatmap showing phosphorylation of indicated genes as determined by reverse phase protein array (RPPA). (**d**) AP-1- GFP reporter plasmid was transfected into WT and *Mir22*$^{-/-}$ BMDCs and GFP intensity was quantitated by flow cytometry 24 hours after αCD40 activation. **, $p<0.01$, unpaired t-test. (n=3–4)

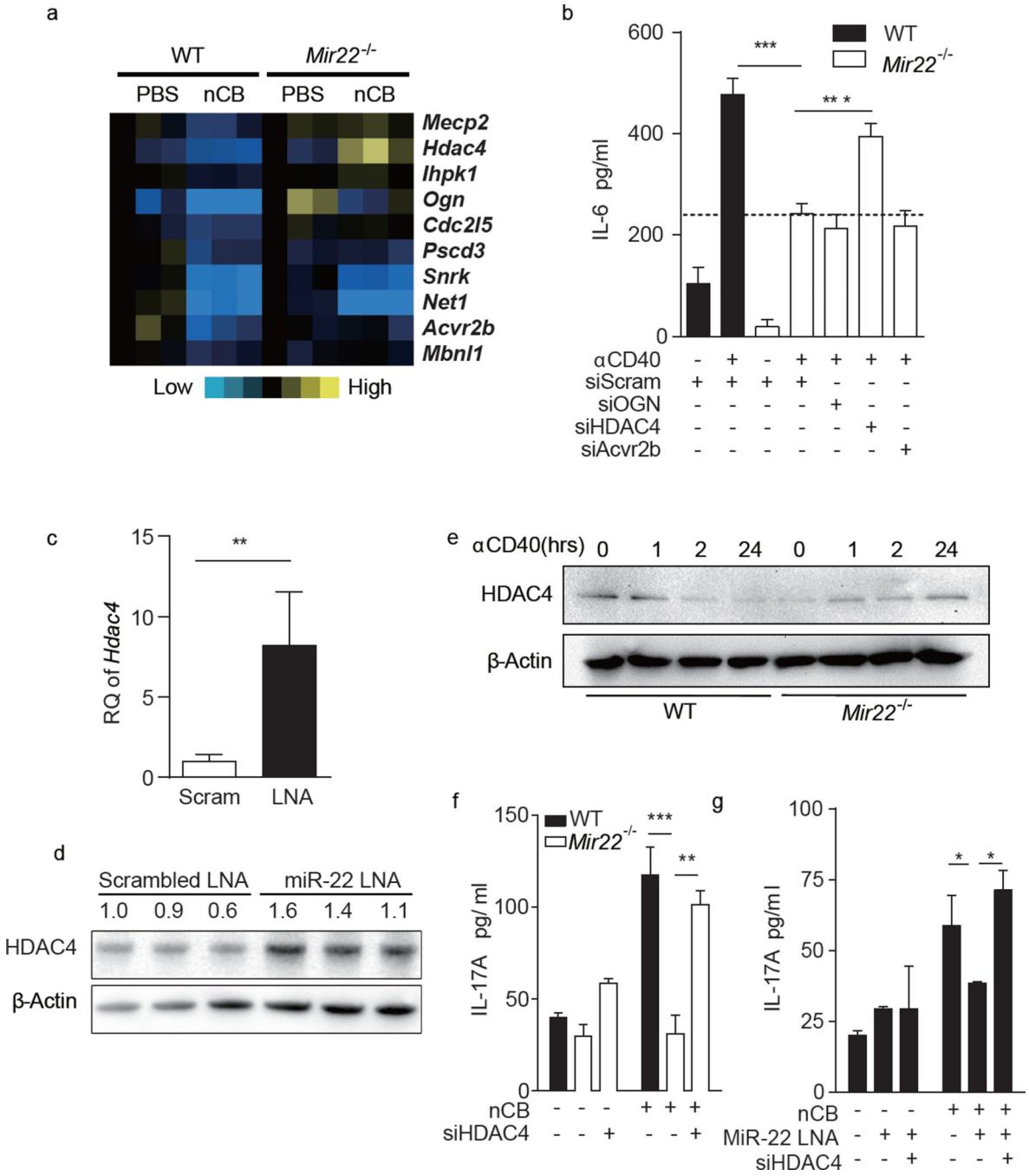

Figure 6.

MiR-22 targets HDAC4 in APCs to promote IL-6 production. (**a**) Heat map depicting changes in the expression of miR-22 predicted target genes in wild type (WT) and *Mir22*$^{-/-}$ CD11c^{+} APCs stimulated with either vehicle (PBS) or nCB (Carbon). (**b**) WT or *Mir22*$^{-/-}$ BMDCs were transfected with either scrambled control siRNA or indicated gene specific siRNAs and were stimulated with αCD40 antibody overnight. IL-6 production was measured by ELISA (n=5). (**c,d**) WT BMDCs were transfected with scrambled LNA (Scram) or miR-22 antisense LNA (miR-22 LNA). Expression of HDAC4 mRNA (**c**, n=3,

RQ: relative quantity to 18S) and protein (**d**) were determined by RT-qPCR and immunoblot. Numbers indicate the HDAC4/β-actin density ratio. (**e**) WT or *Mir22*$^{-/-}$ BMDCs were stimulated with αCD40 antibody for the indicated time (hrs) and HDAC4 expression was determined by immunoblot. (**f**) WT and *Mir22*$^{-/-}$ BMDCs were transfected with scrambled or HDAC4 siRNA (siHDAC4). (**g**) WT BMDCs were transfected with scrambled, miR-22 antisense LNA (MiR-22 LNA) and/or HDAC4 siRNA (siHDAC4). All BMDCs were primed with or without 1000ng nCB and co-cultured with WT naïve CD4^{+} T cells for 3 days and secreted IL-17A was measured by ELISA (n=4). *: $p<0.05$; **: $p<0.01$; ***: $p<0.001$, Unpaired t-test (**c**) and Kruskal Wallis tests (**b,f,g**). Data in (**b**-**g**) are from one of three or four comparable experiments.

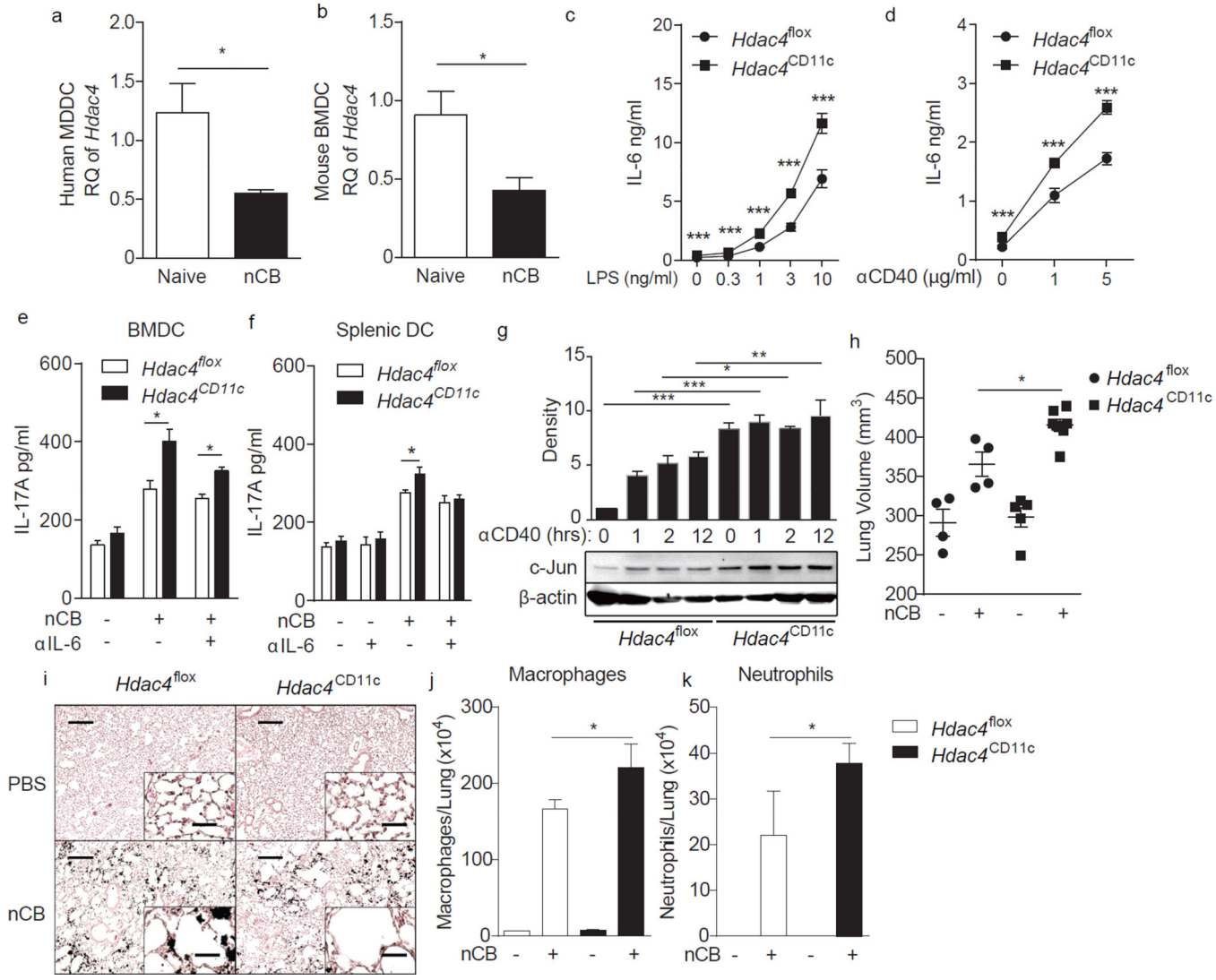

Figure 7.

HDAC4 inhibits APC activation and emphysema progression. (**a,b**) HDAC4 expression in human monocyte derived dendritic cells (**a**) and mouse BMDCs (**b**) before and after stimulation with 1000ng nCB (n=4). RQ: relative quantity to 18S. (**c-e**) BMDCs generated from CD11c–specific conditional HDAC4 deletion mice (*Hdac4*^{CD11c}) and control mice carrying HDAC4-loxp alleles (*Hdac4*^{flox}) were stimulated with LPS (**c**) or αCD40 (**d**) overnight. Secreted IL-6 (**c,d**) was quantitated by ELISA (n=4–5). (**e,f**) HDAC4 deficient BMDCs (**e**) or splenic DCs (**f**) were primed with or without 1000ng nCB and co-cultured with WT naïve CD4^{+} T cells for 3 days and secreted IL-17A was measured by ELISA (n=4–5). (**g**) Expression of c-Jun in HDAC4 deficient BMDCs treated with αCD40 at different time points was determined by immunoblot. Representative blot shown at bottom and the top bar graph shows cumulative density measurements of each band from three comparable experiments. (**h–k**) *Hdac4*^{CD11c} and *Hdac4*^{flox} mice were challenged with nCB for one month. (**h**) Micro-CT quantification of lung volume. (**i**) Representative H&E stained lung sections (of 4 total; 50× magnification; insets: 400×; Scale bars: 200 μm; insets: 25 μm).

Macrophages (**j**) and neutrophils (**k**) in BALF. *: $p<0.05$; **: $p<0.01$; ***: $p<0.001$, Mann Whitney (**a–f**) and Kruskal Wallis tests (**g,h,j–k**). Data in are from one of three comparable experiments.

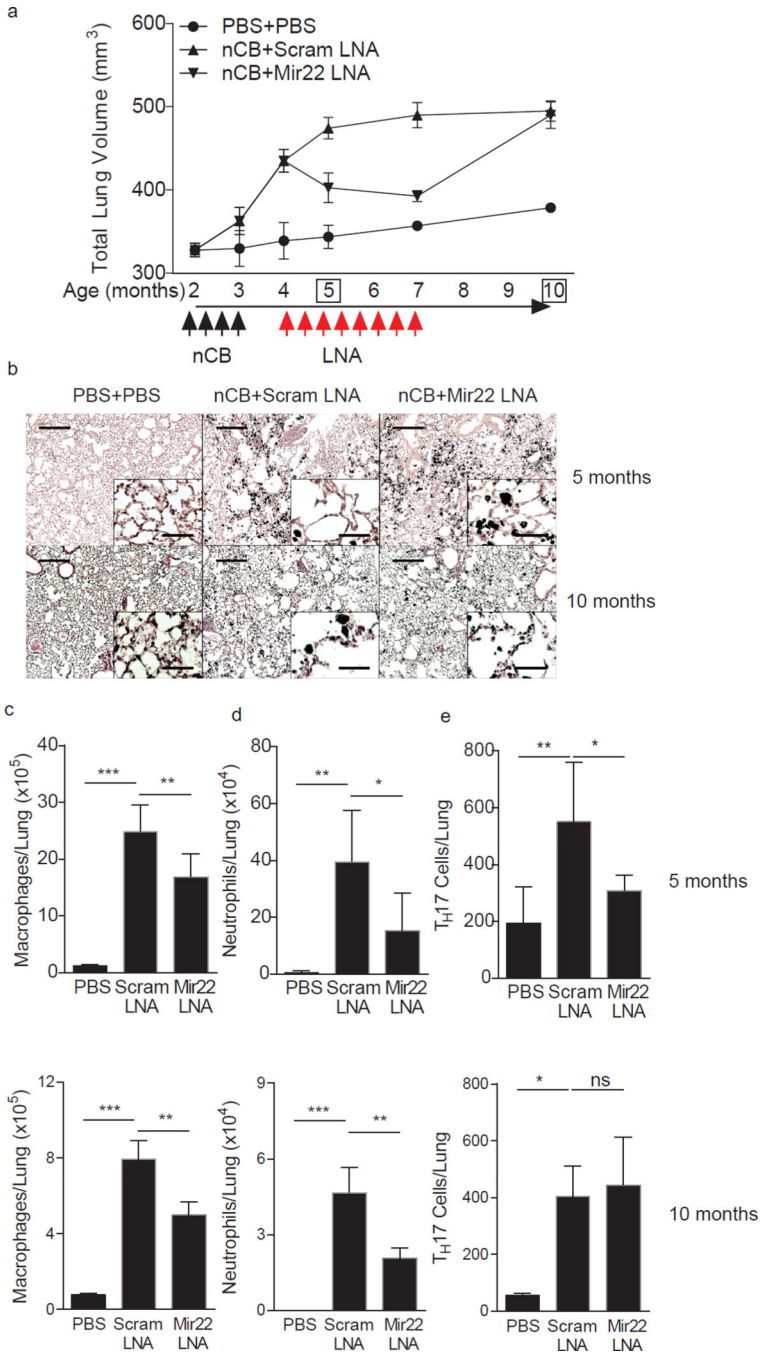

Figure 8.

Neutralizing lung miR-22 reverses nCB-induced emphysema. (**a**) Protocol for intranasal administration of nCB and LNA in relation to microCT scanning to monitor disease progression. (**b–e**) Mice were sacrificed at 5 and 10 months. (**b**) Representative H&E stained lung sections (of 4 total; 50 × magnification; insets: 400×; scale bars: 200 μm; insets: 25 μm). Macrophage (**c**) and neutrophil (**d**) abundance in bronchoalveolar lavage fluid and total

lung T_H17 cells (**e**) as assessed by flow cytometry. *, $p<0.05$; **, $p<0.01$; ***, $p<0.001$, Kruskal Wallis test (n=4–6). Data are from one of three comparable experiments.